The SHDRA syndrome associated gene TMEM260 encodes a protein-specific O-mannosyltransferase

Ida Larsen
University of Copenhagen
Lorenzo Povolo
University of Copenhagen https://orcid.org/0000-0001-7927-823X
Luping Zhou
University of Marburg
Weihua Tian
University of Copenhagen
Kasper Mygind
University of Copenhagen
John Hintze
University of Copenhagen
Chen Jiang
University of Marburg
Verity Hartill
University of Leeds
Katrina Prescott
Chapel Allerton Hospital
Colin Johnson
Sureni Mullegama
GeneDx
Allyn McConkie-Rosell
Duke University Medical Center
Marie McDonald
Duke University Medical Center
Lars Hansen
University of Copenhagen
Sergey Vakhrushev
University of Copenhagen https://orcid.org/0000-0002-0418-5765
Katrine Schjoldager
University of Copenhagen
Henrik Clausen
University of Copenhagen https://orcid.org/0000-0002-0915-5055

Thomas Worzfeld
University of Marburg https://orcid.org/0000-0003-3908-403X
Hiren Joshi
University of Copenhagen
Adnan halim (halim@sund.ku.dk)
University of Copenhagen https://orcid.org/0000-0003-1629-187X

Research Article

Keywords:

Posted Date: May 13th, 2022

DOI: https://doi.org/10.21203/rs.3.rs-1615826/v1

The SHDRA syndrome associated gene *TMEM260* encodes a protein-specific O-mannosyltransferase

Ida Signe Bohse Larsen[1], Lorenzo Povolo[1], Luping Zhou[2], Weihua Tian[1], Kasper Mygind[1], John Hintze[1], Chen Jiang[2], Verity Hartill[3,4], Katrina Prescott[4], Colin A. Johnson[3], Sureni V. Mullegama[5], Allyn McConkie-Rosell[6], Marie McDonald[6], Lars Hansen[1], Sergey Vakhrushev[1], Katrine T. Schjoldager[1], Henrik Clausen[1], Thomas Worzfeld[2,7], Hiren J. Joshi[1]*, Adnan Halim[1]*

Affiliations:

[1]Copenhagen Center for Glycomics, Department of Cellular and Molecular Medicine, University of Copenhagen, Denmark.

[2]Institute of Pharmacology, Faculty of Medicine, University of Marburg, Marburg, Germany.

[3]Leeds Institute of Medical Research, University of Leeds, St James' University Hospital, Leeds. UK.

[4]Yorkshire Regional Genetics Service, Chapel Allerton Hospital, Leeds, UK

[5]GeneDx, Gaithersburg, MD, USA

[6]Division of Medical Genetics, Duke University Medical Center, North Carolina, USA.

[7]Max-Planck-Institute for Heart and Lung Research, Bad Nauheim, Germany

*Corresponding authors. Email: joshi@sund.ku.dk or halim@sund.ku.dk

Abstract: Mutations in the *TMEM260* gene cause structural heart defects and renal anomalies syndrome (SHDRA), but the function of the encoded protein remains unknown. We report that TMEM260 is an ER-located protein O-mannosyltransferase that selectively glycosylates defined extracellular immunoglobulin, plexin, transcription factor (IPT) domains of the hepatocyte growth factor receptor (cMET), macrophage-stimulating protein receptor (RON), and plexin receptors. We demonstrate that disease-causing *TMEM260* mutations impair O-mannosylation of IPT domains and that *TMEM260* knock out in cells results in receptor maturation defects and abnormal growth of 3D cell models. Thus, our study identifies a new, receptor-specific O-mannosylation pathway that serves critical functions during epithelial morphogenesis.

One-Sentence Summary: Mutations in *TMEM260* disrupt functional O-mannosylation of receptors

Main text

The autosomal recessive congenital disorder SHDRA (OMIM: 617478) is caused by bi-allelic mutations in *TMEM260* (**Fig. S1, Table S1**) (*1, 2*), a gene without known function encoding a predicted multi-pass transmembrane protein. We identified *TMEM260* in a bioinformatic screen for putative multi-pass transmembrane glycosyltransferases using the Pfam database. The predicted domain structure of TMEM260 shows similarity (**Fig. 1A, Fig. S2**) to protein O-mannosyltransferases POMT1 and POMT2 (*3*), for which deficiencies cause different forms of muscular dystrophy-dystroglycanopathies (MDDG) (*4, 5*), and the more recently discovered transmembrane and tetratricopeptide repeat-containing proteins 1-4 (TMTC1-4) (*6*), for which deficiencies in TMTC3 cause cobblestone lissencephaly (*7*), and other TMTCs are associated with periventricular nodular heterotopia with intellectual disability and epilepsy (*8*), and hearing loss (*9*).

The POMT1-2 and TMTC1-4 protein O-mannosyltransferases glycosylate different classes of protein clients (*10*). POMT1-2 transfer O-linked mannose (O-Man) to alpha-dystroglycan (αDG) of the dystrophin-glycoprotein complex (DGC) where elongated complex O-Man glycans on αDG mediate interactions between extracellular matrix (ECM) proteins, the DGC, and the cellular cytoskeleton (*11*). The TMTC1-4 family transfer O-Man to the extracellular cadherin (EC) domains of the cadherin superfamily, including E- and N-cadherin and clustered/non-clustered protocadherins (*6, 12, 13*). We previously described a third class of O-mannosylated proteins characterized by extracellular immunoglobulin, plexin, transcription factor (IPT) domains (**Fig. 1B**), which were not dependent on the functions of POMT1-2 and TMTC1-4 (*6, 10*). Thus, the identification of TMEM260 as a potential O-Man glycosyltransferase prompted us to investigate if TMEM260 is responsible for O-Man glycosylation of extracellular IPT domains and whether clinically relevant *TMEM260* mutants influence O-Man biosynthesis in cell models.

Transient expression of TMEM260-3xFLAG in human breast cancer BG1 cells demonstrated that TMEM260 is localized to the endoplasmic reticulum (ER) (**Fig. S3**), akin to POMT1-2 and TMTC1-4 enzymes (*14, 15*), and proteomic analysis of the affinity purified TMEM260-3xFLAG protein revealed high-mannose type N-glycan on Asn569, thus confirming that the C-terminal domain of TMEM260 faces the ER lumen (**Fig. S4**). To assess whether TMEM260 is directly involved in protein O-glycosylation, we employed human HEK293

SimpleCells (HEK293^{SC}) with knockout (KO) of *COSMC* and *POMGNT1* genes involved in biosynthesis of complex O-glycans, which enables simple enrichment of O-Man glycopeptides by Concanavalin A (ConA) lectin chromatography (*12*). The HEK293^{SC} cells were further engineered to establish KO of *TMEM260* (HEK293$^{SC/KO:TMEM260}$) and total cell extracts from both cell lines were encoded by stable isotopes before quantitative O-Man glycoproteome analyses as previously described (*6, 13*). Mass spectrometry-based relative quantification of O-Man glycopeptides revealed that *TMEM260* KO selectively affected glycopeptides derived from IPT domains of plexins (plexin A1-4, B1-2 and D1), hepatocyte growth factor receptor (cMET), and the macrophage-stimulating protein receptor (RON) (**Fig. 1B-C, Data S1**). This subclass of single pass (type I) transmembrane receptors share structural similarities, including a common extracellular domain structure consisting of a Sema domain, PSI domains (plexins, semaphorins, and integrins), and 3-4 IPT domains (*16, 17*). However, plexin, cMET and RON are functionally diverse receptors that regulate a multitude of development processes including epithelial organization, neural patterning and morphogenesis of the heart, kidney, and skeletal system (*18-21*). Notably, *TMEM260* KO did not influence O-Man glycosylation of αDG or cadherins, which are known substrates of POMT1-2 and TMTC1-4 enzymes, respectively (**Fig. 1C**). KO of *TMEM260* in wild-type HEK293 cells (HEK293$^{KO:TMEM260}$) further confirmed the selective loss of O-Man glycans on IPT domains (**Fig. 1C**), and conversely, reintroduction of *TMEM260* by site-directed knock-in (KI) in HEK293$^{KO:TMEM260}$ cells specifically rescued IPT domain O-Man glycosylation (**Fig. 1C**). These results thus indicate that TMEM260 is a protein-specific O-mannosyltransferase that targets O-Man to extracellular IPT domains found among a distinct class of cell-surface receptors.

To gain further structural insight, we expressed a full-length cMET-3xFLAG fusion protein in HEK293^{WT} and HEK293$^{SC/KO:TMEM260}$ cells and confirmed TMEM260 dependent O-Man glycosylation of β-strands in three IPT domains (**Fig. S5**). Label-free quantification demonstrated high O-Man occupancy at Thr582 (68%), Thr676 (100%; fully occupied) and Thr761 (44%) in the mature cMETβ chain expressed in HEK293^{WT} (**Fig. S5**). The O-Man glycans of IPT domains were sensitive to jack bean alpha-mannosidase digestion, thus demonstrating that the linkage is in α-anomeric configuration (**Fig. S5**). Furthermore, we utilized the open search MS Fragger tool (*22*) for unbiased mining of MS/MS data but found

no evidence of complex O-Man glycans on IPT domains (**Fig. S6**), thus indicating that TMEM260-specific O-Man glycans are not elongated into complex structures.

The SHDRA syndrome caused by mutations in the *TMEM260* gene (*1, 2*) was predicted to have relative high carrier frequency in select populations with ranges from 0.0007-0.007 across ancestries. To confirm that predicted deleterious mutations affected the O-Man glycosylation function, we analyzed two reported homozygous *TMEM260* mutations c.1393C>T, p.Q465* (*1*); c.1698_1701del, p.Y567Tfs*27, (*1*), and two novel homozygous variants c.293 G>A, p.C98Y and c.1357T>C, p. C453R identified in two affected families (**Fig 1A, Fig. S1**). Western blot analyses indicated that all TMEM260 variants expressed but were unstable in comparison to the wild-type protein (**Fig. 1D**). Furthermore, KI of these variants revealed markedly reduced ability to rescue and induce O-Man glycosylation on extracellular IPT domains in HEK293$^{KO:TMEM260}$ cells (**Fig. 1C**), verifying that the glycosylation function of TMEM260 is impaired. Interestingly, the *TMEM260* variants from the two newly identified families presenting milder phenotypes (**Table S1**) and carrying homozygous C98Y or C453R substitutions (**Fig. S1, Table S1**), appeared to exhibit some degree of rescue of enzyme function, as evidenced by the differential O-Man glycoproteomic analysis (**Fig. 1C**).

We next investigated the endogenous cMET, RON and Plexin-B2 receptors in human breast cancer BG1$^{KO:\textit{TMEM260}}$ cells by Western blot analysis and confirmed that maturation of the cMET receptor was not influenced by *TMEM260* KO (**Fig. 2A**). However, proteolytic maturation of both RON and Plexin-B2 was partly affected, with accumulation of the pro-forms in total cell lysates (**Fig. 2A**). Immunofluorescence cytology revealed that Plexin-B2 accumulated in ER with marked reduction in cell surface expression in BG1$^{KO:\textit{TMEM260}}$ cells (**Fig. 2B**). Flow cytometry analysis further confirmed that cell surface expression of cMET was unaffected by loss of O-mannosylation, while cell surface expression of RON and Plexin-B2 receptors were markedly reduced in BG1$^{KO:\textit{TMEM260}}$ cells (**Fig. 2C**).

Plexin receptors are important for controlled cell division and normal growth in epithelial cells (*23, 24*). Considering the renal defects found in patients with *TMEM260* deficiencies (*1*), we turned to a 3D spheroid model using mouse inner medullary duct epithelial cells (mIMCD-3) (*25*) and introduced KO of *Tmem260* (**Table S2 and S3**). Differential glycoproteomic analyses of mIMCD-3$^{KO:Tmem260}$ cells confirmed selective loss of O-Man

glycosylation in IPT domains of cMET and plexin A1, -B1, -B2 and D1 receptors (**Data S1**). Using two independent clones each of mIMCD-3^{WT} and mIMCD-3$^{KO:Tmem260}$ cells, we found that mIMCD-3^{WT} produced normal spheroids with properly formed lumina and cellular junctions based on apical ZO-1 expression and adherence junctions visualization by E-cadherin immunofluorescence staining, while mIMCD-3$^{KO:Tmem260}$ cells produced spheroids with profound growth and architectural defects (**Fig. 3A**). The mIMCD-3^{WT} cell clones formed an average of 76% and 70% normal cysts, whereas only 20% and 11% of the mIMCD-3$^{KO:Tmem260}$ clones formed normal cysts (**Fig. 3B**). The mIMCD-3$^{KO:TMEM260}$ spheroids (average area of 2.7 mm^2 and 2.9 mm^2) were notably larger in size compared to mIMCD-3^{WT} spheroids, which had an average area of 1.0 mm^2 (**Fig. 3C**), and we further noted that mIMCD-3$^{KO:Tmem260}$ spheroids showed increased number of nuclei per cyst, with an average 46 and 38 nuclei versus 10 and 13 nuclei for mIMCD-3^{WT} (**Fig. 3D**). These findings indicate that TMEM260-directed O-mannosylation of IPT domains is critical for receptor functions and normal epithelial morphogenesis.

In conclusion, we identified the function of TMEM260, underlying the syndrome SHDRA, as a protein-specific O-mannosyltransferase targeting cMET, RON and plexin receptors, thus establishing SHDRA as a new member of the expanding group of congenital disorders of glycosylation (CDGs) (*26, 27*). The *TMEM260* gene is conserved in metazoans and SHDRA phenotypes are recapitulated by *tmem260* KO in *D. rerio* (*1*), suggesting that this novel type of O-mannosylation is important for development in metazoans. Truncus arteriosus (TA), a rare congenital heart defect consistently observed in individuals with biallelic mutations in *TMEM260 (2)*, is a prominent phenotype of *plexinD1*$^{-/-}$ mice (*28*), which may indicate dysfunctional Plexin-D1 signaling in affected individuals (*2*) and further studies are clearly warranted. Our discovery of the TMEM260-directed O-mannosylation pathway expands the known types of distinct protein glycosylation pathways in mammals to a total of 14 (*29*) and demonstrates that protein O-mannosylation is widely used in mammalian cells. Interestingly, protein O-mannosylation, once considered to be restricted to yeast (*3, 14*), has evolved to three distinct types in metazoans (and one type of C-mannosylation (*30*)), to differentially serve highly distinct classes of proteins and biological functions (*10, 29*). Our enhanced knowledge of different types of protein glycosylation pathways is also providing a conceptual advance, where an increasing number of pathways appear to be dedicated to specific protein folds and classes of proteins compared to the more classical types of N-

glycosylation and GalNAc-type O-glycosylation that are rather ubiquitously found on proteins (*29*).

References and Notes

1. A. Ta-Shma *et al.*, Mutations in TMEM260 Cause a Pediatric Neurodevelopmental, Cardiac, and Renal Syndrome. *Am J Hum Genet* **100**, 666-675 (2017).
2. A. T. Pagnamenta *et al.*, Biallelic TMEM260 variants cause truncus arteriosus, with or without renal defects. *Clin Genet* **101**, 127-133 (2022).
3. L. Lehle, S. Strahl, W. Tanner, Protein glycosylation, conserved from yeast to man: a model organism helps elucidate congenital human diseases. *Angew Chem Int Ed Engl* **45**, 6802-6818 (2006).
4. D. Beltran-Valero de Bernabe *et al.*, Mutations in the O-mannosyltransferase gene POMT1 give rise to the severe neuronal migration disorder Walker-Warburg syndrome. *Am J Hum Genet* **71**, 1033-1043 (2002).
5. J. van Reeuwijk *et al.*, POMT2 mutations cause alpha-dystroglycan hypoglycosylation and Walker-Warburg syndrome. *J Med Genet* **42**, 907-912 (2005).
6. I. S. B. Larsen *et al.*, Discovery of an O-mannosylation pathway selectively serving cadherins and protocadherins. *Proc Natl Acad Sci U S A* **114**, 11163-11168 (2017).
7. J. Jerber *et al.*, Biallelic Mutations in TMTC3, Encoding a Transmembrane and TPR-Containing Protein, Lead to Cobblestone Lissencephaly. *Am J Hum Genet* **99**, 1181-1189 (2016).
8. S. M. K. Farhan *et al.*, Identification of a novel synaptic protein, TMTC3, involved in periventricular nodular heterotopia with intellectual disability and epilepsy. *Hum Mol Genet* **26**, 4278-4289 (2017).
9. J. Li *et al.*, Deletion of Tmtc4 activates the unfolded protein response and causes postnatal hearing loss. *J Clin Invest* **128**, 5150-5162 (2018).
10. I. S. B. Larsen, Y. Narimatsu, H. Clausen, H. J. Joshi, A. Halim, Multiple distinct O-Mannosylation pathways in eukaryotes. *Curr Opin Struct Biol* **56**, 171-178 (2019).
11. T. Yoshida-Moriguchi, K. P. Campbell, Matriglycan: a novel polysaccharide that links dystroglycan to the basement membrane. *Glycobiology* **25**, 702-713 (2015).
12. M. B. Vester-Christensen *et al.*, Mining the O-mannose glycoproteome reveals cadherins as major O-mannosylated glycoproteins. *Proc Natl Acad Sci U S A* **110**, 21018-21023 (2013).
13. I. S. B. Larsen *et al.*, Mammalian O-mannosylation of cadherins and plexins is independent of protein O-mannosyltransferases 1 and 2. *J Biol Chem* **292**, 11586-11598 (2017).
14. S. Strahl-Bolsinger, M. Gentzsch, W. Tanner, Protein O-mannosylation. *Biochim Biophys Acta* **1426**, 297-307 (1999).
15. J. C. Sunryd *et al.*, TMTC1 and TMTC2 are novel endoplasmic reticulum tetratricopeptide repeat-containing adapter proteins involved in calcium homeostasis. *J Biol Chem* **289**, 16085-16099 (2014).

16. T. Worzfeld, S. Offermanns, Semaphorins and plexins as therapeutic targets. *Nat Rev Drug Discov* **13**, 603-621 (2014).
17. P. Bork, T. Doerks, T. A. Springer, B. Snel, Domains in plexins: links to integrins and transcription factors. *Trends Biochem Sci* **24**, 261-263 (1999).
18. Y. W. Zhang, G. F. Vande Woude, HGF/SF-met signaling in the control of branching morphogenesis and invasion. *J Cell Biochem* **88**, 408-417 (2003).
19. S. Artigiani, P. M. Comoglio, L. Tamagnone, Plexins, semaphorins, and scatter factor receptors: a common root for cell guidance signals? *IUBMB Life* **48**, 477-482 (1999).
20. H. Khoury *et al.*, HGF converts ErbB2/Neu epithelial morphogenesis to cell invasion. *Mol Biol Cell* **16**, 550-561 (2005).
21. A. Maeshima, Y. Q. Zhang, M. Furukawa, T. Naruse, I. Kojima, Hepatocyte growth factor induces branching tubulogenesis in MDCK cells by modulating the activin-follistatin system. *Kidney Int* **58**, 1511-1522 (2000).
22. D. A. Polasky, F. Yu, G. C. Teo, A. I. Nesvizhskii, Fast and comprehensive N- and O-glycoproteomics analysis with MSFragger-Glyco. *Nat Methods* **17**, 1125-1132 (2020).
23. J. Xia *et al.*, Semaphorin-Plexin Signaling Controls Mitotic Spindle Orientation during Epithelial Morphogenesis and Repair. *Dev Cell* **33**, 299-313 (2015).
24. C. Jiang *et al.*, Mechanochemical control of epidermal stem cell divisions by B-plexins. *Nat Commun* **12**, 1308 (2021).
25. R. H. Giles, H. Ajzenberg, P. K. Jackson, 3D spheroid model of mIMCD3 cells for studying ciliopathies and renal epithelial disorders. *Nat Protoc* **9**, 2725-2731 (2014).
26. J. Jaeken, Congenital disorders of glycosylation. *Ann N Y Acad Sci* **1214**, 190-198 (2010).
27. B. G. Ng, H. H. Freeze, Perspectives on Glycosylation and Its Congenital Disorders. *Trends Genet* **34**, 466-476 (2018).
28. A. D. Gitler, M. M. Lu, J. A. Epstein, PlexinD1 and semaphorin signaling are required in endothelial cells for cardiovascular development. *Dev Cell* **7**, 107-116 (2004).
29. K. T. Schjoldager, Y. Narimatsu, H. J. Joshi, H. Clausen, Global view of human protein glycosylation pathways and functions. *Nat Rev Mol Cell Biol* **21**, 729-749 (2020).
30. A. Shcherbakova, B. Tiemann, F. F. Buettner, H. Bakker, Distinct C-mannosylation of netrin receptor thrombospondin type 1 repeats by mammalian DPY19L1 and DPY19L3. *Proc Natl Acad Sci U S A* **114**, 2574-2579 (2017).
31. L. A. Lonowski *et al.*, Genome editing using FACS enrichment of nuclease-expressing cells and indel detection by amplicon analysis. *Nat Protoc* **12**, 581-603 (2017).
32. Z. Yang *et al.*, Fast and sensitive detection of indels induced by precise gene targeting. *Nucleic Acids Res* **43**, e59 (2015).
33. R. Pinto *et al.*, Precise integration of inducible transcriptional elements (PrIITE) enables absolute control of gene expression. *Nucleic Acids Res* **45**, e123 (2017).
34. P. J. Boersema, R. Raijmakers, S. Lemeer, S. Mohammed, A. J. Heck, Multiplex peptide stable isotope dimethyl labeling for quantitative proteomics. *Nat Protoc* **4**, 484-494 (2009).
35. J. Jung *et al.*, Deuterium-Free, Three-Plexed Peptide Diethylation for Highly Accurate Quantitative Proteomics. *J Proteome Res* **18**, 1078-1087 (2019).
36. Y. Perez-Riverol *et al.*, The PRIDE database resources in 2022: a hub for mass spectrometry-based proteomics evidences. *Nucleic Acids Res* **50**, D543-D552 (2022).
37. K. Retterer *et al.*, Assessing copy number from exome sequencing and exome array CGH based on CNV spectrum in a large clinical cohort. *Genet Med* **17**, 623-629 (2015).

38. M. Lommel, A. Schott, T. Jank, V. Hofmann, S. Strahl, A conserved acidic motif is crucial for enzymatic activity of protein O-mannosyltransferases. *J Biol Chem* **286**, 39768-39775 (2011).
39. M. B. Lazarus, Y. Nam, J. Jiang, P. Sliz, S. Walker, Structure of human O-GlcNAc transferase and its complex with a peptide substrate. *Nature* **469**, 564-567 (2011).

Acknowledgments:

Funding: This work was supported by VILLUM FONDEN grant 00025438 (AH), Mizutani Foundation for Glycoscience (AH), Danish National Research Foundation grant DNRF107 (HC), Lundbeck Foundation (ISBL), Sir Jules Thorn Biomedical Award JT/09 (CAJ), MRC/NIHR CARP fellowship MR/V037617/1 (VH), British Heart Foundation clinical research fellowship FS/13/32/30069 (VH), the Deutsche Forschungsgemeinschaft grant GRK 2213 (TW), and the China Scholarship Council grant 201908080171 (LZ). We thank Francis Jacob (University Hospital Basel) for providing BG1 cells and Maxwell L. Bileschi (Google Research, Cambridge, USA) for discussion and analysis of protein domains.

Author contributions:

Conceptualization: ISBL, HC, TW, HJJ, AH.

Methodology: ISBL, LP, LZ, JH, CJ, HC, TW, HJJ, AH.

Investigation: ISBL, LP, LZ, WT, KM, JH, CJ, VH, KP, CAJ, SVM, AMR, MM, LH, SV, KTS, HJJ, AH.

Visualization: ISBL, LP, KM, LZ, TW, AH

Funding acquisition: ISBL, LZ, VH, CAJ, KTS, HC, TW, AH.

Project administration: AH

Supervision: KTS, HC, TW, HJJ, AH.

Writing – original draft: AH

Writing – review & editing: ISBL, LP, LZ, WT, KM, JH, VH, CAJ, SVM, AMR, LH, KTS, HC, TW, HJJ, AH

Competing interests: Dr. Mullegama is an employee of GeneDx, Inc. All other authors declare that they have no competing interests.

Data and materials availability: All cell lines are available on request under standard materials transfer agreements (MTAs) with University of Copenhagen for academic research purposes. The mass spectrometry proteomics data have been deposited to the ProteomeXchange Consortium via the PRIDE partner repository with the dataset identifier PXD032328.

Figure legends

Fig. 1. Mutations in TMEM260 abolish O-mannosylation of IPT domains. (**A**) Graphical depiction of predicted domain structure of TMEM260 and the known protein O-mannosyltransferases. TMEM260 is predicted to contain 11 TM helixes and a C-terminal domain in the ER-lumen. Protein coordinates of clinical mutations in TMEM260 are indicated with filled red circles. POMT1/2 contain 11 transmembrane (TM) helixes and MIR domains facing the ER-lumen. TMTC1-4 contain 11 TM helixes and C-terminal tetratricopeptide (TPR) repeats in the ER-lumen. (**B**) IPT domains of cMET, RON and plexin receptors are O-Man glycosylated on evolutionary conserved Thr/Ser residues. (**C**) Differential O-Man glycoproteomic analysis of HEK293 cell lines with knock-out (KO) and/or knock-in (KI) of TMEM260 variants. Scatter plots with $\log_{10}$ fold change (ratio of >1 represents loss of O-mannosylation) of glycopeptide abundances in HEK293 KO/KI total cell lysates for POMT1/2 substrates (DAG1, KIAA1549, SUCO), TMTC1-4 substrates (EC-domains) and TMEM260 substrates (IPT domains). (**D**) Western blot analysis of $HEK293^{WT}$, $HEK293^{KO:TMEM260}$ and $HEK293^{KO:TMEM260}$ cells stably expressing 3xFLAG-tagged *TMEM260* WT or mutant genes.

Fig. 2. Loss of TMEM260 O-mannosylation leads to protein maturation defects. (**A**) Western blot analysis of total cell lysates of $BG1^{WT}$ and $BG1^{KO:TMEM260}$ cells showing accumulation of larger pro-forms (arrow) of RON and plexin-B2, but not cMET, in *TMEM260* KO cells. Bar graphs show average values for quantification by densitometric analysis of pro- and mature forms over the total intensity (pro-form + mature). The analysis was performed in triplicates for $BG1^{WT}$, $BG1^{KO:TMTC3}$ (control) and three clones of $BG1^{KO:TMEM260}$. (**B**) Immunofluorescence analysis of $BG1^{WT}$ and $BG1^{KO:TMEM260}$ cells demonstrates retention of plexin-B2 in ER. (**C**) Flow cytometry analysis and quantification of cell-surface expression of cMET, RON and plexin-B2 receptors in $BG1^{WT}$, $BG1^{KO:TMTC3}$ (control) and $BG1^{KO:TMEM260}$ cells (KO clones #1, #2 and #3), showing reduced cell-surface expression of RON and plexin-B2. Statistical analyses were performed by one-way ANOVA, Tukey test.

Fig. 3. Loss of *Tmem260* impairs mIMCD-3 spheroid formation. (**A**) Brightfield images ("BF"; scale bar, 100 µm) of mIMCD-3^{WT} (clones #1 and #2) and mIMCD-$3^{KO:Tmem260}$ cells (clones #1 and #2) cultured in matrigel for 3 days. Representative confocal images of anti-E-cadherin (green) and anti-ZO-1 (red) immunostaining are shown (scale bar, 15 µm). Blue: DAPI. (**B**) Quantification of the percentage of normal cysts based on E-cadherin and ZO-1 immunostaining (n=3 independent experiments); asterisk (*) indicates $p<0.0001$. (**C**)

Quantification of cyst size based on E-cadherin and ZO-1 immunostaining (n=3 independent experiments); **p=0.0008 for WT #1 vs. KO #1, *p=0.0005 for WT #1 vs. KO #2, **p=0.0008 for WT #2 vs. KO #1, *p=0.0005 for WT #2 vs. KO #2. (**D**) Quantification of cell numbers per cyst based on DAPI staining (n=3 independent experiments); *p=0.0025 for WT #1 vs. KO #1, ***p=0.0106 for WT #1 vs. KO #2, **p=0.0044 for WT #2 vs. KO #1 or 2, ****p=0.0206 for WT #2 vs. KO #2. Statistical analysis was performed by one-way ANOVA, Tukey test.

Figure 1

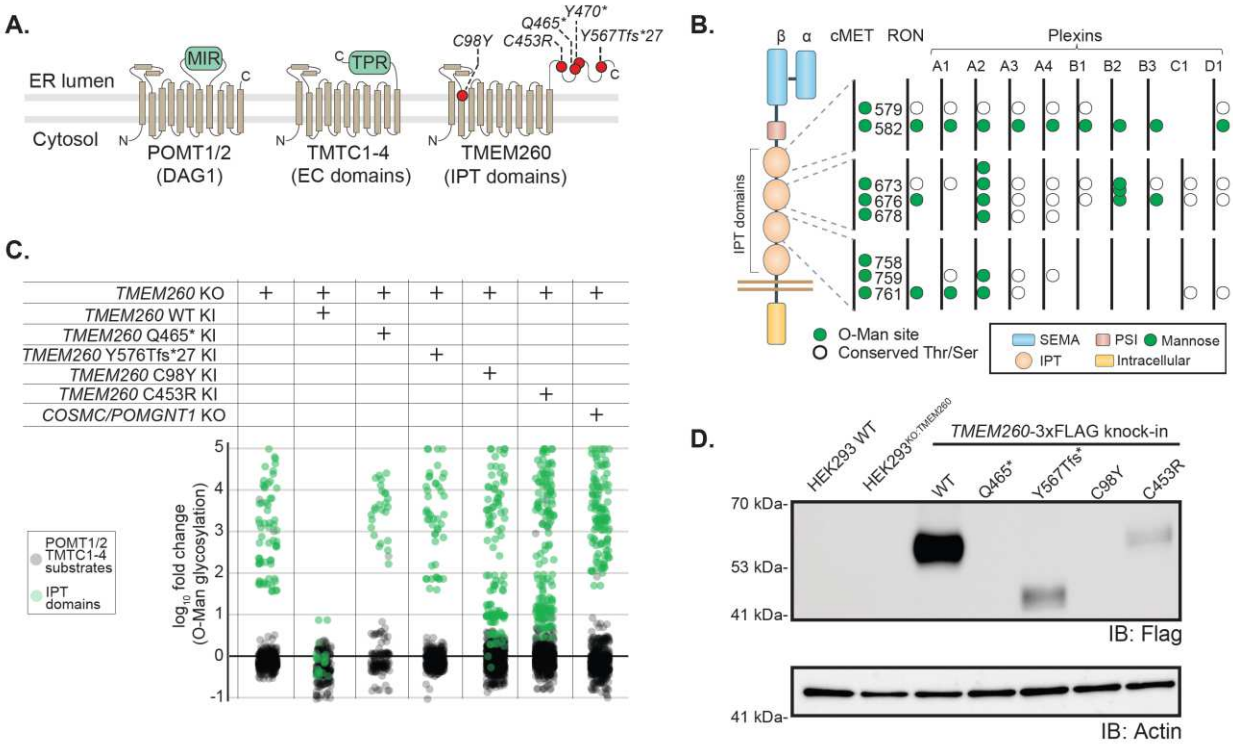
A.
ER lumen
Cytosol
MIR
TPR
C98Y
C453R
Q465*
Y470*
Y567Tfs*27
POMT1/2
(DAG1)
TMTC1-4
(EC domains)
TMEM260
(IPT domains)
B.
β
α
cMET
RON
Plexins
A1
A2
A3
A4
B1
B2
B3
C1
D1
IPT domains
579
582
673
676
678
758
759
761
O-Man site
Conserved Thr/Ser
SEMA
PSI
Mannose
IPT
Intracellular
C.
TMEM260 KO
TMEM260 WT KI
TMEM260 Q465* KI
TMEM260 Y576Tfs*27 KI
TMEM260 C98Y KI
TMEM260 C453R KI
COSMC/POMGNT1 KO
POMT1/2 TMTC1-4 substrates
IPT domains
log10 fold change (O-Man glycosylation)
D.
HEK293 WT
HEK293 KO TMEM260
TMEM260-3xFLAG knock-in
WT
Q465*
Y567Tfs*
C98Y
C453R
70 kDa-
53 kDa-
41 kDa-
IB: Flag
41 kDa-
IB: Actin

Figure 2

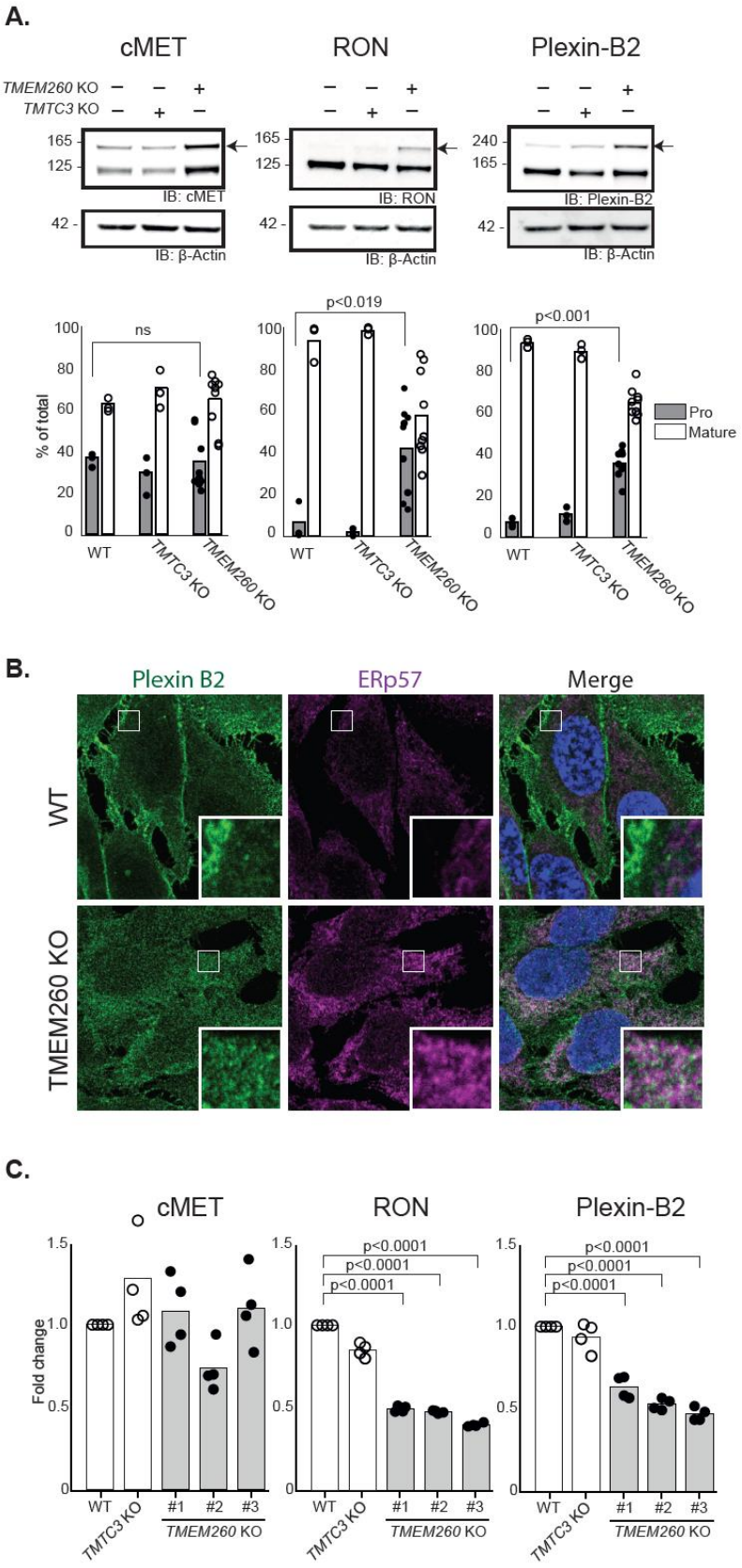
A.
cMET
RON
Plexin-B2
TMEM260 KO
TMTC3 KO
IB: cMET
IB: RON
IB: Plexin-B2
IB: β-Actin
ns
p<0.019
p<0.001
% of total
Pro
Mature
WT
TMTC3 KO
TMEM260 KO
B.
Plexin B2
ERp57
Merge
WT
TMEM260 KO
C.
cMET
RON
Plexin-B2
Fold change
p<0.0001
#1
#2
#3

Figure 3

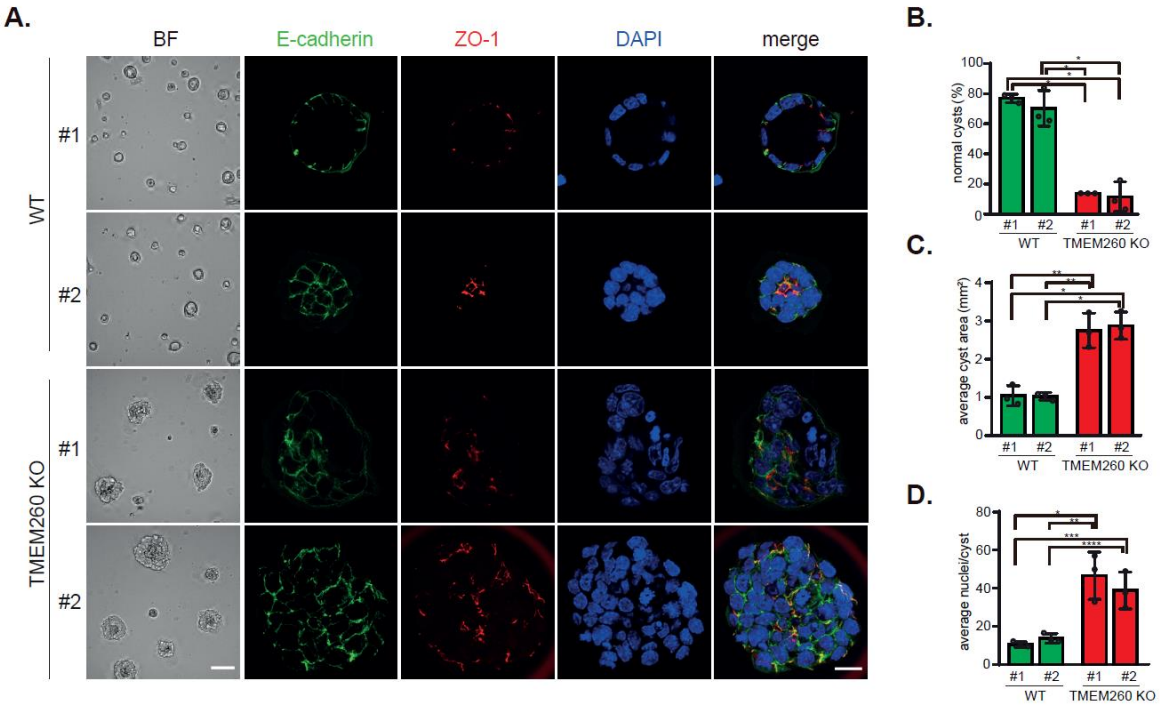
A.
BF
E-cadherin
ZO-1
DAPI
merge
WT
TMEM260 KO
#1
#2
B.
normal cysts (%)
C.
average cyst area (mm²)
D.
average nuclei/cyst
WT
TMEM260 KO

Supplementary Information for

The SHDRA syndrome associated gene *TMEM260* encodes a protein-specific O-mannosyltransferase

Ida Signe Bohse Larsen[1], Lorenzo Povolo[1], Luping Zhou[2], Weihua Tian[1], Kasper Mygind[1], John Hintze[1], Chen Jiang[2], Verity Hartill[3,4], Katrina Prescott[4], Colin A. Johnson[3], Sureni V. Mullegama[5], Allyn McConkie-Rosell[6], Marie McDonald[6], Lars Hansen[1], Sergey Vakhrushev[1], Katrine T. Schjoldager[1], Henrik Clausen[1], Thomas Worzfeld[2,7], Hiren J. Joshi[1]*, Adnan Halim[1]*

Correspondence to: joshi@sund.ku.dk or halim@sund.ku.dk

This PDF file includes:

Materials and Methods
Supplementary Text
Figs. S1 to S6
Tables S1 to S5
Captions for Data S1
References 31-39

Other Supplementary information for this manuscript include the following:

Data S1

Materials and Methods

Cell culture

BG1 cells were cultured in RPMI 1640 medium (Sigma) supplemented with 10% FBS (Gibco) and 1% GlutaMAX (Gibco). HEK293 cells were cultured in DMEM medium (Gibco) supplemented with 10% FBS (Gibco) and 1% GlutaMAX (Gibco). mIMCD-3 cells (*25*) were cultured in DMEM/F12 medium (Gibco) supplemented with 10% FBS (Gibco) and 1% GlutaMAX (Gibco).

Gene editing, constructs design, Knock-in and Knock-out

To generate knock-out (KO) cell lines, guide-RNAs (gRNAs) were designed targeting the *TMEM260* gene in mouse and human genomes. The gRNAs were cloned into EPB104-pU6 (Addgene #68369). KO clones were generated according to published protocol (*31, 32*). Briefly, cells were seeded in 6-well plates, transfected the following day with 1.5 µg of PBKS-Cas9-2A-eGFP plasmid (Addgene #68371) and 1 µg gRNA plasmid using Lipofectamine 3000. eGFP positive cells were FACS-enriched 24h after transfection and single-cell sorted after one week. KO clones were identified by Indel Detection by Amplicon Analysis (IDAA) (*32*), and validated by sanger sequencing (Table S2-S4). Generation of KI clones was performed as previously published (*33*), and based on the ObLiGaRe strategy targeting the safe harbor AAVS1 site in human cell lines. The donor plasmid pAAVS1 Insulator ObLiGaRe/EPB71 was designed and synthesized by Genewiz, USA (Addgene #90018), and contains CMV-gene of interest-polyA. The full-length TMEM260-3xFLAG WT sequence of donor plasmid was commercially synthesized and cloned in the donor plasmid by Genewiz, USA, while patient mutations were introduced by site-directed plasmid mutagenesis. Mutations Q465* and Y567Tfs*27 were generated using InFusion DNA polymerase (TaKaRa) and C98Y and C453R using KOD DNA polymerase (Sigma-Aldrich), followed by DpnI (NEB) digestion of donor plasmid and transformation in Stellar competent cells (TaKaRa). For WB analysis, two additional plasmids encoding TMEM260(Q465*)-3xFLAG and TMEM260(Y567Tfs*27)-3xFLAG were generated from the donor constructs using primers in Table S4. All plasmids were confirmed by Sanger Sequencing and a total of seven *TMEM260* variant constructs were used for stable cell lines generation. HEK293 *TMEM260* KO cells were used as parental strain to generate *TMEM260* variant KI cell lines. In brief, 3 µg of donor plasmid and 1.5 µg of each AAVS1 CompoZr ZFN plasmids (Sigma) encoding ZFN1/2-2A-GFP/E2-Crimson (*33*) were co-transfected in TMEM260 KO cells using Lipofectamine 3000 (Thermo) according to manufacturer's protocol. One day after transfection, cells expressing both GFP and E2-Crimson were enriched by FACS (Sony Cell Sorter SH800S) as previously described (*33*). After one week, bulk populations were single-cell sorted in 96-well plates. Correct stable genomic integration was confirmed using junction PCR of A) the region between the 5' of AAVS1 genomic locus upstream of the ZFNs cutting site and the 3' end of the donor construct B) the region between the 5' end of the donor construct and the 3' of AAVS1 genomic locus downstream of the ZFNs cutting site.

Dimethyl labelling of HEK293 total cell digests for differential glycoproteomics

Sample preparation was performed as previously described (*6, 34*) with minor modifications. Approximately 0.5 mL packed cell pellets were lysed in 1 mL 0.1% RapiGest SF Surfactant (Waters) in 50 mM ammonium bicarbonate by incubation on ice and probe sonication. Protein extract was separated from insoluble material by centrifugation (1000 g, 10 min), reduced (10 mM dithiothreitol, 37°C, 30 min) and alkylated (25 mM iodoacetamide, RT, 30 min) before

digestion with 25 µg trypsin at 37°C, 16h (Roche). Tryptic digests were labelled with stable dimethyl isotopes using light- or medium dimethyl labels on C18 Sep-Pak columns (Waters) as described (*34*). After dimethylation, tryptic digests were mixed in 1:1 ratio, digested by PNGase F (Sigma, 16U, 37°C, 16 h) in 150 µL 100 mM Tris, pH 7.4 and subjected to Concanavalin A (ConA) lectin weak affinity chromatography (LWAC) as described below.

Diethyl labelling of HEK293 total cell digests for differential glycoproteomics

HEK293 total cell extracts were prepared using S-Trap midi columns (Protifi) with minor modifications to protocol from vendor. Briefly, 0.2 mL packed cells were lysed by probe sonication in 500 µL 5% SDS, 100 mM ammonium bicarbonate. Solution was clarified by centrifugation (13,000 g, 10 min) before reduction (20 mM DTT, 80°C, 10 min) and alkylation (100 mM iodoacetamide, 30 min, RT). Phosphoric acid was added to final concentration of 1.2% (v/v) and mixed with 3.3 mL 100 mM ammonium bicarbonate in 90% methanol. The solution was applied to the S-Trap column and washed according to vendor's protocol. Trypsin (25 µg in 350 µL 100 mM ammonium bicarbonate) was gently applied and S-Trap column was left at 37°C, 18h. Finally, tryptic peptides were recovered (4,000 g, 1 min) from S-Trap column and pooled with a second 50% acetonitrile, 0.2% formic acid elution (4,000 g, 1 min). Pooled S-Trap eluates were evaporated to remove organic solvents and further desalted by Sep-Pak C18 (100 mg) cartridges. Desalted peptides from HEK293 cell extracts were dried and labelled with stable diethyl isotopes in light (acetaldehyde) or heavy channels ($^{13}CH_3{}^{13}CHO$, Cambridge Isotope Laboratories) as previously described (*35*). After diethylation, peptides were mixed in 1:1 ratio, digested by PNGase F (16U, 37°C, 16h) in 150 µL 100 mM Tris, pH 7.6 and subjected to ConA LWAC as described below.

TMT labelling of mIMCD-3 total cell digests for differential glycoproteomics

Proteins were extracted and digested with trypsin in 0.1% RapiGest, 50 mM ammonium bicarbonate as described above. Following Sep-Pak C18 desalting, tryptic digests were quantified by Nanodrop 205 nm absorbance. For each channel, 500 µg peptides were reconstituted in 50 mM HEPES, pH 8.0 and labelled with 800 µg tandem mass tags (6-plex TMT kit, Thermo). miMCD-3 WT clone #1 and clone #2 were labelled with TMT-126 and TMT-127, respectively. miMCD-3 Tmem260 KO clone #1 was labelled with TMT-128 and TMT-129. miMCD-3 Tmem260 KO clone #2 was labelled with TMT-130 and TMT-131. Labelling efficiency and mixing was evaluated by mass spectrometry. The final 6-plex labelled tryptic peptide mixture (3 mg) was digested with PNGase F as described above and subjected to ConA LWAC as described below.

Concanavalin A lectin weak affinity chromatography (ConA LWAC)

PNGase F treated and stable isotope labelled tryptic peptides were diluted to 1.5-2 mL with ConA running buffer (25 mM Tris, pH 7.4, 300 mM NaCl, 0.5 mM $MgCl_2$, 0.5 mM $MnCl_2$) and loaded on a 3-meter column packed in-house with ConA-agarose beads (Vector Laboratories). Chromatography was operated at 100 µL/min. Non-glycosylated peptides were collected in the flow-through fraction and the column was washed with running buffer until UV signal was below 5 mAU. O-Man glycopeptides were eluted with 0.5M methyl-α-D-mannopyranoside in running buffer. Elution fractions were desalted by in-house packed Stage tips (Empore disk-C18, 3M) before mass spectrometry.

Conjugation of mouse M2 antibody to Dynabeads M-270 epoxy

1 mL of mouse M2 antibody (1mg/mL, F1804-5MG, Sigma-Alrich) was buffer exchanged into 0.1M sodium phosphate, pH 7.4, using 2 mL Zebaspin columns (#89889, Thermo Fischer Scientific) and mixed with 500 uL 3M ammonium sulfate in 0.1M sodium phosphate, pH 7.4. The antibody solution was mixed with 50 mg of pre-washed (2x2mL 0.1M sodium phosphate, pH 7.4) Dynabeads M-270 epoxy (#14302D, Thermo Fisher Scintific) and incubated with rotation at 30°C (20-24h). The conjugated beads were subsequently washed with 4x2 mL PBS, 2x2 mL 0.5% Triton X-100 in PBS and finally in 2x2 mL PBS. The beads were stored up to 3 months at 4°C in 330 uL (~150 ug/uL) 10% glycerol, 0.02% NaN_3 in PBS.

Immunoprecipitation of cMET and glycosidase treatment

300 µL packed cell pellets from cells overexpressing cMET-FLAG ($HEK293^{WT}$ cMET-3xFLAG KI and $HEK293^{SC/KO:TMEM260}$ cMET-3xFLAG KI), were lysed in 600µL of extraction buffer (50 mM HEPES, pH 7.4, 50 mM K-Acetate, 200 mM NaCl, 2 mM $MgCl_2$, 1 mM DTT, 0.1% Tween-20, 0.5% Triton X-100), the lysate was cleared at 21.000g, 10 min at 4°C. 600 µL cleared lysate was mixed with 60 µL M2-Dynabeads slurry (described above). The extract and beads were incubated with rotation at 4°C, 45 min. The extract was removed and beads were washed with 3x12mL wash solution (50mM HEPES, pH 7.4, 50 mM K-Acetate, 200mM NaCl, 2mM $MgCl_2$, 1mM DTT, 0.1% Tween-20). Bound proteins were eluted by incubating (10 min shaking, RT) the beads in 25 µL wash solution supplemented with 1 µg/µL FLAG peptide (#F4799, Sigma-Aldrich). The elution was performed twice and supernatants (2x25µL) were pooled.
For glycosidase treatment, 10 µL elution from the immunoprecipitation experiment above was reduced with 10 mM DTT at 37°C and treated with 1 µL PNGase F (#11365177001, Roche) overnight at 37°C. The reaction mixture was diluted with NuPAGE LDS sample buffer (4X, #NP0007, Thermo Fisher Scientific), heated at 72°C, 10 min and separated on a 4-12% BIS-Tris SDS-PAGE gel in MOPS running buffer before staining with Imperial protein stain (#24615, Thermo Fisher Scientific). To investigate cMET O-mannosylation by bottom-up analysis, 30 µL of the elution fractions were evaporated to dryness before reduction (100mM DTT, 60°C, 30 min), alkylation (250mM iodoacetamide, RT, 30 min, protected from light) in 2xLDS buffer and separation on a 4-12% BIS-Tris SDS-PAGE gel. Specific bands migrating at the expected molecular weight of pro-MET and mature cMETβ polypeptide chains were excised. Each gel band was destained by 3x200 µL 50% acetonitrile (ACN) in 100 mM ammonium bicarbonate, 15 min, 37°C, followed by addition of 100% ACN, 10 min, RT, to dehydrate the gel pieces. The gel pieces were soaked in 50 µL 5% ACN, 100mM ammonium bicarbonate containing 0.5 µg trypsin (Roche) at 37°C ON. Following day, 25 µL of 100% ACN, 0.1% formic acid (FA) was added to extract the digested peptides. The extraction was repeated with 2x50 µL 50% ACN, with each incubation at 5 min, RT, before being pooled. The tryptic peptides were dried by speedvac and diethyl stable isotope labelled as described above. Samples immunoprecipitated from $HEK293^{WT}$ were labeled with heavy diethyl ($^{13}CH_3{}^{13}CHO$), while samples from $HEK293^{SC/KO:TMEM260}$ were labelled with light diethyl (CH_3CHO) reagents. Samples were stage-tipped, mixed in equal amounts and subjected to LC-MS/MS.
Jack bean α1-2,3,6 Mannosidase treatment (NEB) was performed on cMET immunoprecipitated from $HEK293^{WT}$ cells. In-gel trypsin digest of bands corresponding to cMETβ were split in two and diethyl labelled with heavy diethyl isotopes (mock treatment) and light diethyl isotopes (mannosidase treated). The samples were combined, stage-tipped and subjected to LC-MS/MS.

Mass spectrometry

Mass spectrometric analysis of O-mannosylated peptides from total cell tryptic digests was carried out as previously described (*6*). Briefly, desalted ConA elution fractions were

individually injected using a EASY-nLC 1000 system (Thermo Fisher Scientific) interfaced via a nanoSpray Flex ion source to an Fusion Tribrid or Fusion Tribrid Lumos mass spectrometer (Thermo Fisher Scientific). The EASY-nLC 1000 was operated using a single analytical column setup (PicoFrit Emitters, 75-µm inner diameter; New Objectives, Woburn, MA) packed in-house with Reprosil-Pure-AQ C18 phase (1.9-µm particle size; Dr. Maisch). Peptides were separated across 120 min at 200 nL/min; gradient elution was achieved by solvent A (0.1% formic acid) and solvent B (acetonitrile, 0.1% formic acid) which was set for 2–20% B for 95 min followed by 20–80% B for 10 min and finally 80% B for 15 min. Precursor MS1 scan (m/z 355–1700) was acquired in the Orbitrap at a resolution setting of 120,000, followed by Orbitrap HCD-MS/MS and ETciD-MS/MS of multiply charged precursors (z = 2–6) in the MS1 spectrum; a minimum MS1 signal threshold of 10,000–50,000 ions was used for triggering data-dependent fragmentation events; MS2 spectra were acquired at a resolution of 60,000 (HCD and ETciD). For bottom-up analyses of in-gel digested samples from immunoprecipitation experiments, a 90 min nanoLC-MS/MS method (200 nL/min) was used. Gradient elution was achieved by solvent A (0.1% formic acid) and solvent B (acetonitrile, 0.1% formic acid) which was set for 2–25% B for 65 min followed by 25–80% B for 10 min and finally 80% B for 15 min. Precursor MS1 scan (m/z 355–1700) was acquired in the Orbitrap at a resolution setting of 120,000, followed by Orbitrap HCD-MS/MS and ETciD-MS/MS of multiply charged precursors (z = 2–6) in the MS1 spectrum; a minimum MS1 signal threshold of 10,000–50,000 ions was used for triggering data-dependent fragmentation events; MS2 spectra were acquired at a resolution of 60,000 (HCD and ETciD).

Data analyses was carried out using Proteome Discoverer 1.4 software (Thermo Fisher Scientific). Data files (.raw) were processed using the Sequest HT or MS Amanda nodes and searched against the canonical human proteome downloaded (January 2013) from the UniProtKB database (http://www.uniprot.org/). Precursor mass tolerance was set to 10 ppm (Sequest HT) or 5 ppm (MS Amanda) and fragment ion mass tolerance to 0.02 Da. Up to 2 missed trypsin (full- and semi-specific) cleavages were allowed. Carbamidomethylation (cysteine: 57.02146 Da), dimethyl (light: 28.0313 Da, medium: 32.0564 Da), diethyl (light: 56.0626 Da, heavy: 60.07602 Da) and TMT (229.1629 Da) modifications of peptide N-termini and lysines set as a fixed modifications. Oxidation (methionine: 15.9949 Da) was set as variable modification. In addition, Hex (162.0528 Da) was set as variable modification for serine and threonine residues. Peptide confidence levels were calculated using the Target Decoy PSM Validator node and results were filtered for high-confidence ($p < 0.01$) identifications only. All O-mannosylated peptide spectral matches were inspected manually to validate the accuracy of the identifications.

Open search was performed via the Fragpipe (v17.1) user interface with MS fragger (v3.4) installed (*22*). The “glyco-O-open-hybrid” method was used; 162.0528 Da and 324.1056 Da masses were included in the Mass Offsets and Y ion masses lists (MS Fragger). The mass spectrometry proteomics data have been deposited to the ProteomeXchange Consortium via the PRIDE (*36*) partner repository with the dataset identifier PXD032328. The data may be accessed using the following; username: reviewer_pxd032328@ebi.ac.uk and password: 7pPu1FvF

Immunoblotting

HEK293 cells (Fig. 1) were grown in DMEM medium (Gibco), 10% FBS and 1% GlutaMAX (Gibco) to 80% confluence while BG1 cells (Fig. 2) were grown in three biological replicates in RPMI medium (Gibco), 10% FBS and 1% GlutaMAX (Gibco) to subconfluence. Cells were lysed on ice in 50mM HEPES pH 7.4, 150mM NaCl and 1% Triton X-100 for 10 minutes. 1X

cOmplete™ Protease Inhibitor Cocktail (Merck) was added in lysis buffer for BG1 cells. Lysates were cleared by centrifugation for 10 min at 4°C and protein amounts were adjusted after BCA assay (#23225, Thermo Scientific) measurements. Equal amounts of protein extracts were separated on a Bis-Tris 4-12% 10-well Mini Protein Gel (Invitrogen) using MOPS (Fig. 1) or MES (Fig. 2) running buffer. Transfer was performed for 11 minutes at 20V to a nitrocellulose membrane using iBlot™ 2 Gel Transfer Device (Thermo Fisher Scientific). Membranes were blocked in a 5% solution of Skim Milk in TBS-T buffer for 2h (Fig. 1) or 30 minutes (Fig. 2) at RT. Antibodies used for blotting were diluted according to Table S5. For all blots, primary antibodies were incubated overnight at 4°C while secondary antibodies were incubated for 1h at RT with gentle agitation. Blots were developed using SuperSignal™ West Pico PLUS Chemiluminescent Substrate (Thermo Scientific) and imaged by ImageQuant™ LAS 4000 (GE Healthcare). 1X ReBlot Plus Strong Antibody Stripping Solution (#2504, Merck Millipore) was used for stripping before β-Actin reprobing of membranes. Densitometry analysis was performed using the Gel Analyser function in ImageJ and expressed by quantifying pro- and mature form intensities over the total intensity (pro-form + mature). Statistical analysis was performed by one-way ANOVA, Tukey test.

Immunofluorescence

BG1 WT and TMEM260 KO cells were grown to 80 % confluence, on 10mm-diameter cover slides, in 24 well plates. The cells were washed once in PBS and fixed with 4% paraformaldehyde for 10 min at RT and quenched with 100mM NH4Cl in PBS for 10 min. Cells were permeabilized with 0.05% Saponin in PBS with 2 mg/mL bovine serum albumin for 10 min. Cells were stained with primary antibody diluted in permeabilization buffer for 1 h at RT (Table S5). Cells were washed and incubated for 1 h with fluorophore-conjugated secondary antibodies (Table S5) and DAPI. Coverslips were mounted on Mowiol (Calbiochem). Image acquisition was performed using LSM710 (Carl Zeiss) confocal microscope. BG1 WT cells were transiently transfected with TMEM260-3xFLAG, using jetPRIME (PolyPlus) according to manufacturer's protocol. Cells were cultured on 10mm-diameter cover slides, in 24 well plates. 50 µL of jetOPTIMUS buffer along with 0.5 µg DNA and 1 µL of jetOPTIMUS reagent were mixed and incubated for 10 min before addition to the cells. Media were changed 6 h after transfection and cells were incubated for 24 h before fixation and staining as described above.

Identification of two novel *TMEM260* disease variants

Family I: A trio whole exome sequencing was performed on family I using samples from the affected child and both parents. Using genomic DNA from the proband and parents, the exonic regions and flanking splice junctions of the genome were captured using the IDT xGen Exome Research Panel v1.0 (Integrated DNA Technologies, Coralville, IA). Massively parallel (NextGen) sequencing was done on an Illumina system with 100bp or greater paired-end reads. Reads were aligned to human genome build GRCh37/UCSC hg19, and analyzed for sequence variants using a custom-developed analysis tool. Additional sequencing technology and variant interpretation protocol has been previously described (*37*). The general assertion criteria for variant classification are publicly available on the GeneDx ClinVar submission page http://www.ncbi.nlm.nih.gov/clinvar/submitters/26957/). A homozygous variant in TMEM260 (c.293 G>A p C98Y) was identified. No other variants were reported. Additional genetic testing included Array CGH, testing for the FMR1 expanded CGG repeat, were normal.

Family II: Whole exome sequencing was performed using SureSelect Human All Exon V6 (Agilent Technologies) using DNA samples extracted from peripheral blood from the affected

individual, an unaffected sibling and both parents. Libraries were sequenced on an Illumina HiSeq 3000 instrument with 6 samples pooled per lane. Reads were aligned to GRCh37 reference genome using Novoalign (Novocraft Technologies, Selangor, Malaysia). Data analysis was performed assuming a homozygous mutation as the most likely cause of disease. Genome Analysis Toolkit (GATK) HaplotypeCaller was used for variant calling and Ensembl Variant Effect Predictor (VEP) for variant annotation. CNV analysis of WES data was performed using the Exome Depth program in the affected individual. A homozygous TMEM260 variant; 14:57088379T>C, p.C453R, was identified in the affected child and was heterozygous in both parents. In silico tools were supportive of pathogenicity and the CADD score was 25.7. The variant was rare in the Gnomad database (2 of 249420 alleles, no homozygotes). Two other rare homozygous variants were recognised in the affected individual (in SULT4A1 and C2Orf88), neither of which could be linked to the phenotype. Segregation of the variant identified in *TMEM260* was confirmed using conventional Sanger sequencing as homozygous in the affected individual, and heterozygous in both parents and an unaffected sibling.

Supplementary Text

Clinical reports

Family I

Family I is of Native American (Lumbee tribe) origin. There is no known consanguinity in the family. The affected child is a 5 years old male, who presented at birth with complex congenital heart defect. He was born at 39 weeks, birth weight 3.225 kg (40.08%, z – 0.25), Length (53 cm, Z -1.53) HC: 35 cm (49% (Z = -0.02) with Apgars of 7 (1 minute) and 9 (5 minutes). Shortly after birth, he was diagnosed with truncus arteriosus type II with an interrupted aortic arch type B, aberrant R subclavian, and thymic hypoplasia. On examination, no dysmorphic features were noted, he presented nevis anemicus and a supraumbilical raphe, with normal eye and hearing examination. Brain MRI was normal. Kidneys are large for age bilaterally with pelvicaliectasis of the left kidney (Society fetal urology grade 2 hydronephrosis). Otherwise, the kidneys have a normal appearance. He has global developmental delays, did not sit until 1 year, walked at age two years. At 5 years he is nonverbal, does not yet use sign language or other augmentative communication devices and has been diagnosed with autism. He is small for age at 5 years his with height 106.5 cm (4 %, Z= -1.71) and weight 15.2 kg (<1 %, Z= -2.59). Head circumference, at last measurement, age 4 years was 50 cm (40 % (Z= -0.25)

Family II

Family II is of Pakistani origin, where parents are first cousins. Their first child was affected with truncus arteriosus and critical aortic stenosis. She died at day 2 of life due to her severe cardiac phenotype. The second affected child was a male born at 31 weeks gestation by emergency caesarean section. His birth weight was 1.65kg. He had truncus arteriosus, which was diagnosed antenatally, and with ventricular septal defect, atrial septal defect, and tricuspid stenosis at birth. He had deterioration in renal function at 2 weeks of age, although this resolved, and a renal ultrasound scan at that time showed a degree of nephrocalcinosis bilaterally, but no other abnormalities. He suffered from necrotizing enterocolitis in the newborn period. A cranial ultrasound scan at one month of age was normal. He had cardiac surgery at 2 months of age. He had failure to thrive and gastro-oesophageal reflux disease in the first few months of life. He had oral aversion and was NG fed until 2 years of age. He had a gastrostomy placed at the age of 2.5 years. This was removed at the age of 4.5 years. He still has some difficulties with oral intake and needs lots of encouragement to eat and drink. He is now maintaining his weight. He has some mild dysmorphism, including low-set ears. He had global developmental delay, he first sat independently at 8 months and walked at 2.5 years. He had some speech delay and first started speaking at 3.5 years. At the age of 3.5 years his head circumference was 49cm (2nd centile) and height 93cm (<2nd centile). At the age of 7.5 years he is managing in a mainstream school without additional help. He can read and write, but has a short attention span and some disruptive behaviors. His Array CGH was normal.

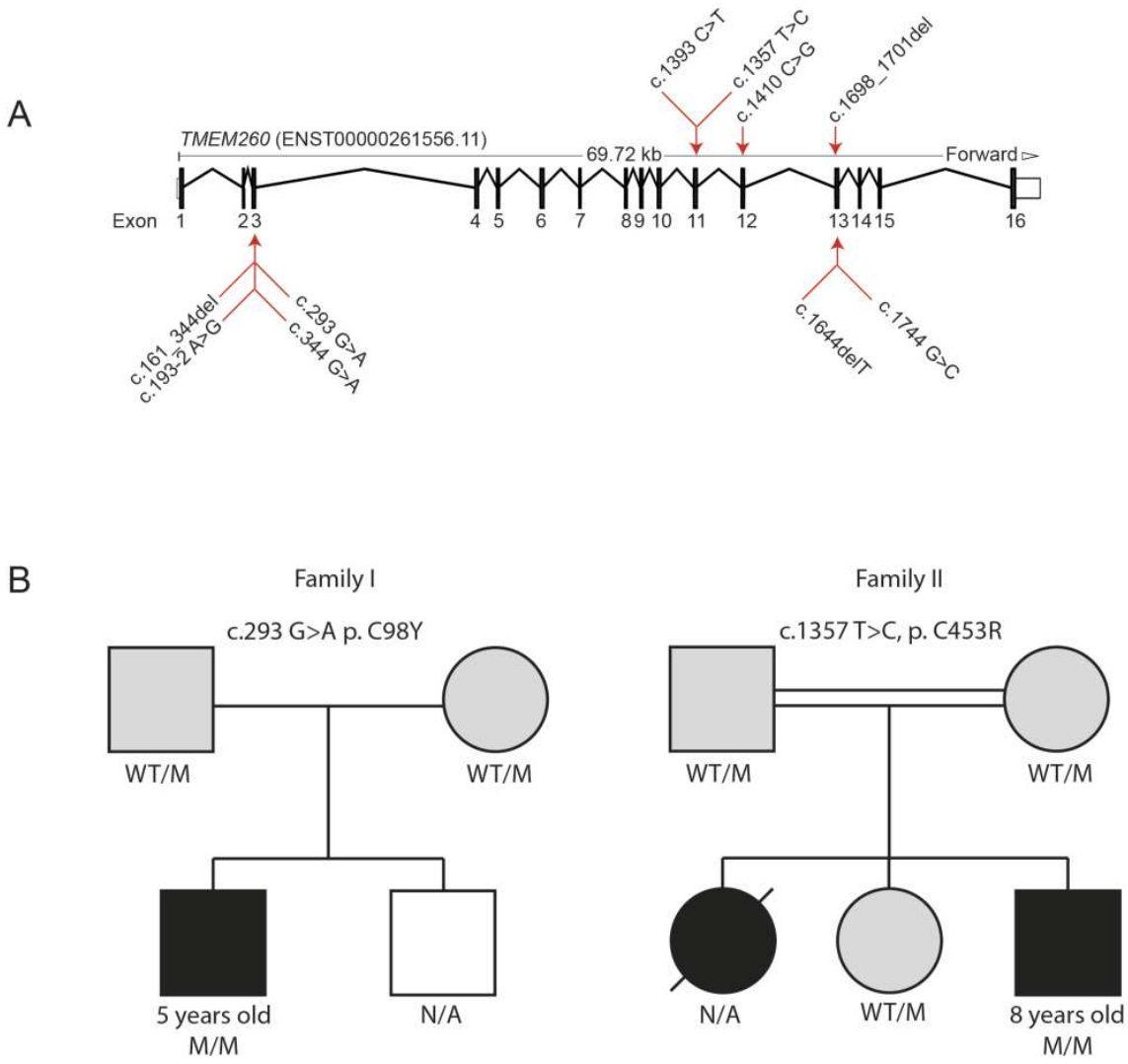

Fig. S1.

Distribution of clinical mutations in TMEM260. **(A)** The cDNA coordinates (red arrows) above and below exons indicate homozygous and heterozygous mutations, respectively. **(B)** Pedigrees of two new and unrelated families identified with homozygous mutations in *TMEM260*. Affected individuals are indicated with black squares (male) and circles (female), unaffected heterozygote individuals are indicated by grey squares (male) and circles (female), unaffected unknown genotypes are indicated as white squares (male) and diagonal line indicate deceased individual. N/A indicates not available.

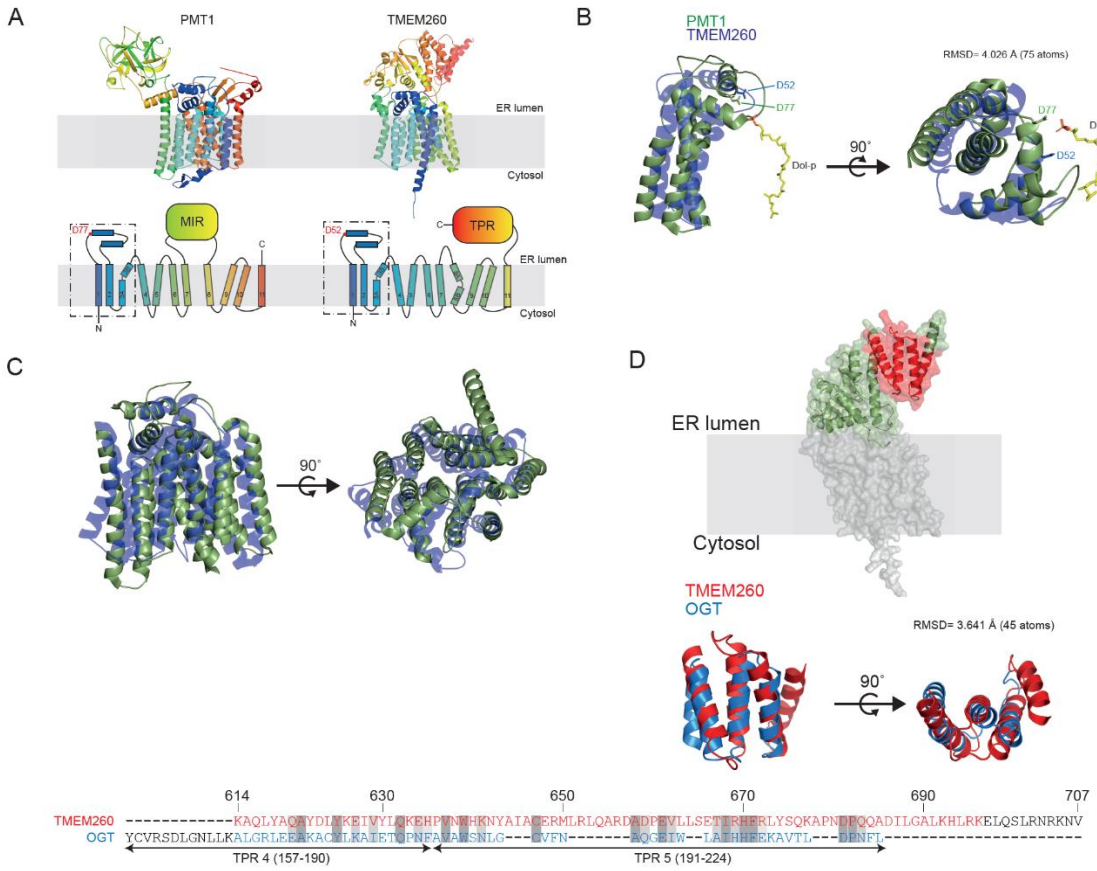

Fig. S2.

TMEM260 shares structural similarity with known O-Man glycosyltransferases. **(A)** The structure of yeast PMT1 (PDB: 6P2R) with 11 transmembrane helixes and MIR-domains in the ER lumen is shown (left) together with the predicted (AlphaFold) structure of TMEM260 (right). The topology and organization of transmembrane helixes and domains in the ER lumen are depicted below PMT1 and TMEM260, respectively. The first loop of PMT1, with the catalytically important D77 (red) residue (*38*) is indicated, which corresponds to D52 in the predicted TMEM260 structure. **(B)** Structural alignment of an amino-terminal segment indicated as a dashed box in (A), including the first three transmembrane helixes and the catalytically important loop of PMT1 (green) demonstrates that the corresponding segment of TMEM260 (transparent blue) aligns well with RMSD=4.026 Å (75 atoms). This structural alignment further shows that D52 of TMEM260 is positioned in the same orientation and space as the critical D77 of PMT1. The co-purified lipid-linked donor Dolichol-phosphate (Dol-p) of PMT1 is shown in yellow/red. **(C)** Structural alignment of the 11 transmembrane helixes of PMT1 (green) and amino-terminal domain (residues 1-410) of TMEM260 (transparent blue), which are predicted to encompass 11 transmembrane helixes that are superimposable with the transmembrane domain of PMT1. **(D)** The predicted structure of the carboxy-terminal domain (residues 411-707) of TMEM260 is shown in green, together with a predicted tetratricopeptide repeat (TPR) domain (residues 614-696) highlighted in red. Sequence and structural alignment of TPR repeats of TMEM260 (red) and O-GlcNAc transferase (*39*) (OGT; blue) is shown for comparison.

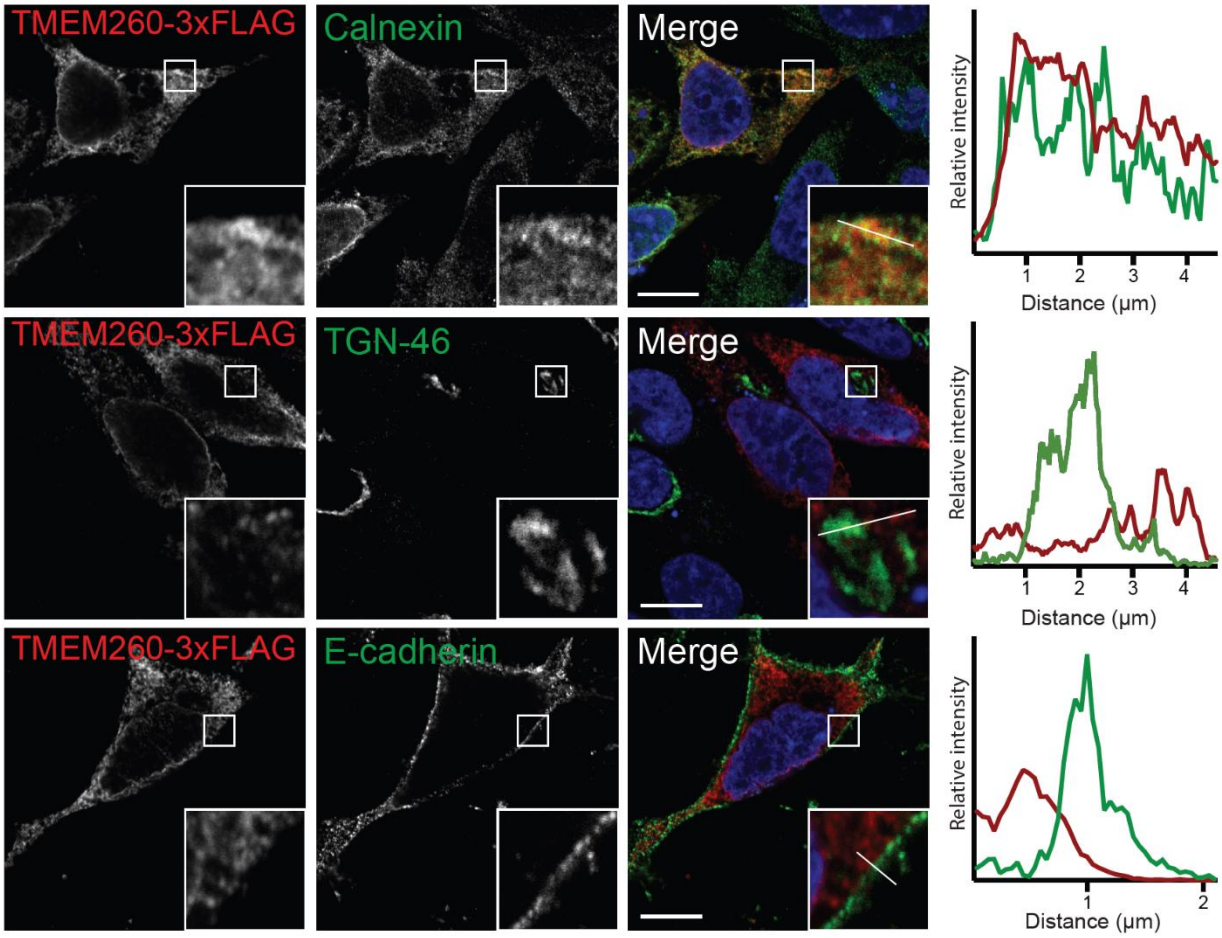

Fig. S3.
TMEM260 is localized in the endoplasmic reticulum. TMEM260-3xFLAG was transiently expressed in BG1 cells and visualized by immunofluorescence. Sub-cellular localization of TMEM260 with ER (Calnexin), Golgi (TGN-46) and cell-surface (E-cadherin) markers demonstrate that TMEM260 resides in the ER compartment. Scale-bar: 10 μm.

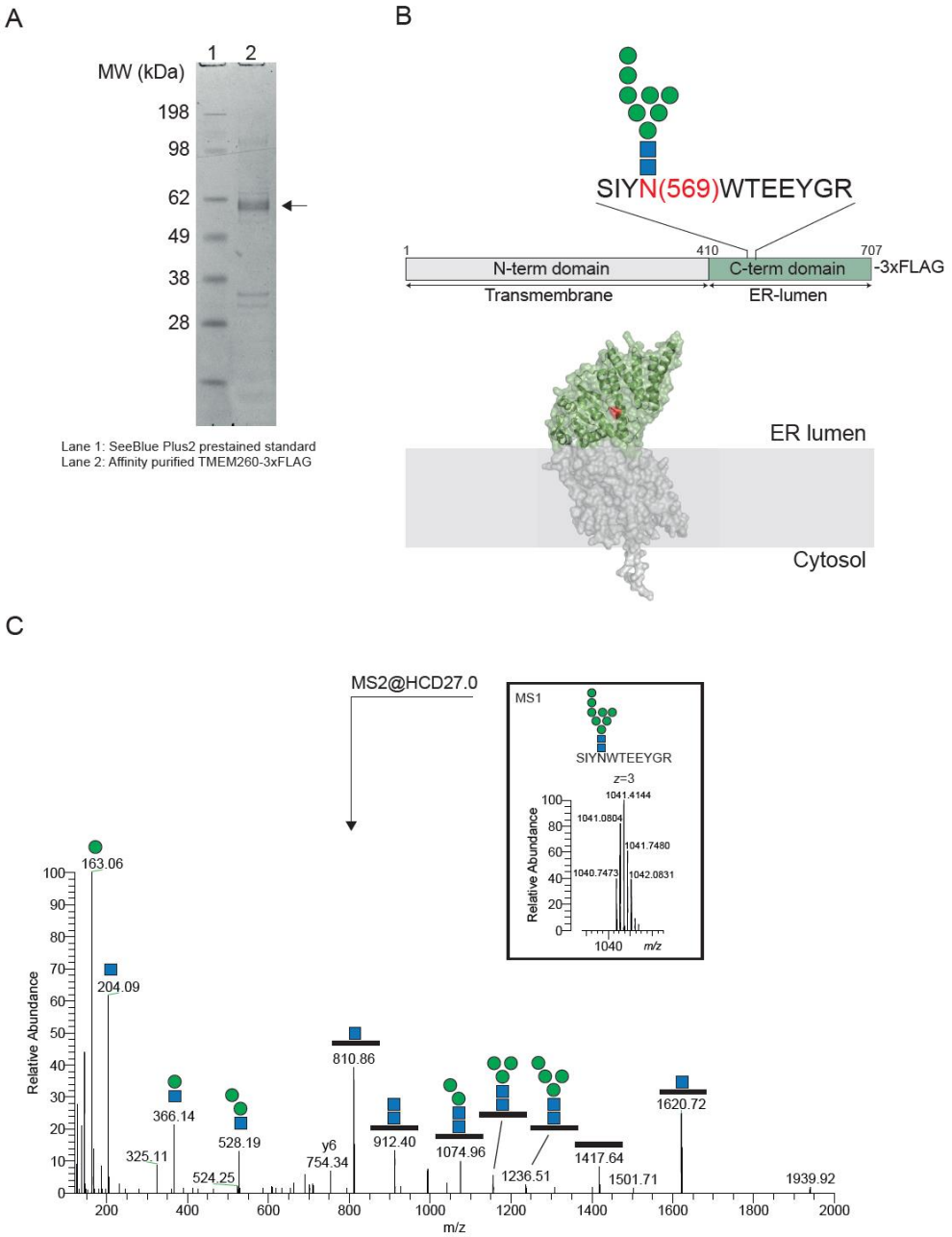

Fig. S4.

The carboxy-terminal domain of TMEM260 is oriented into the ER lumen. **(A)** TMEM260-3xFLAG expressed and affinity purified (arrow) from HEK293 cells. **(B)** Identification of a tryptic glycopeptide with a high mannose-type N-glycan on Asn569. The predicted structural fold of the carboxy-terminal domain is shown in green and the Asn569 residue is indicated in red. **(C)** The glycopeptide precursor ion (box) selected for HCD-MS2 fragmentation is shown together with the annotated fragment ions that identify the glycan- and peptide sequences.

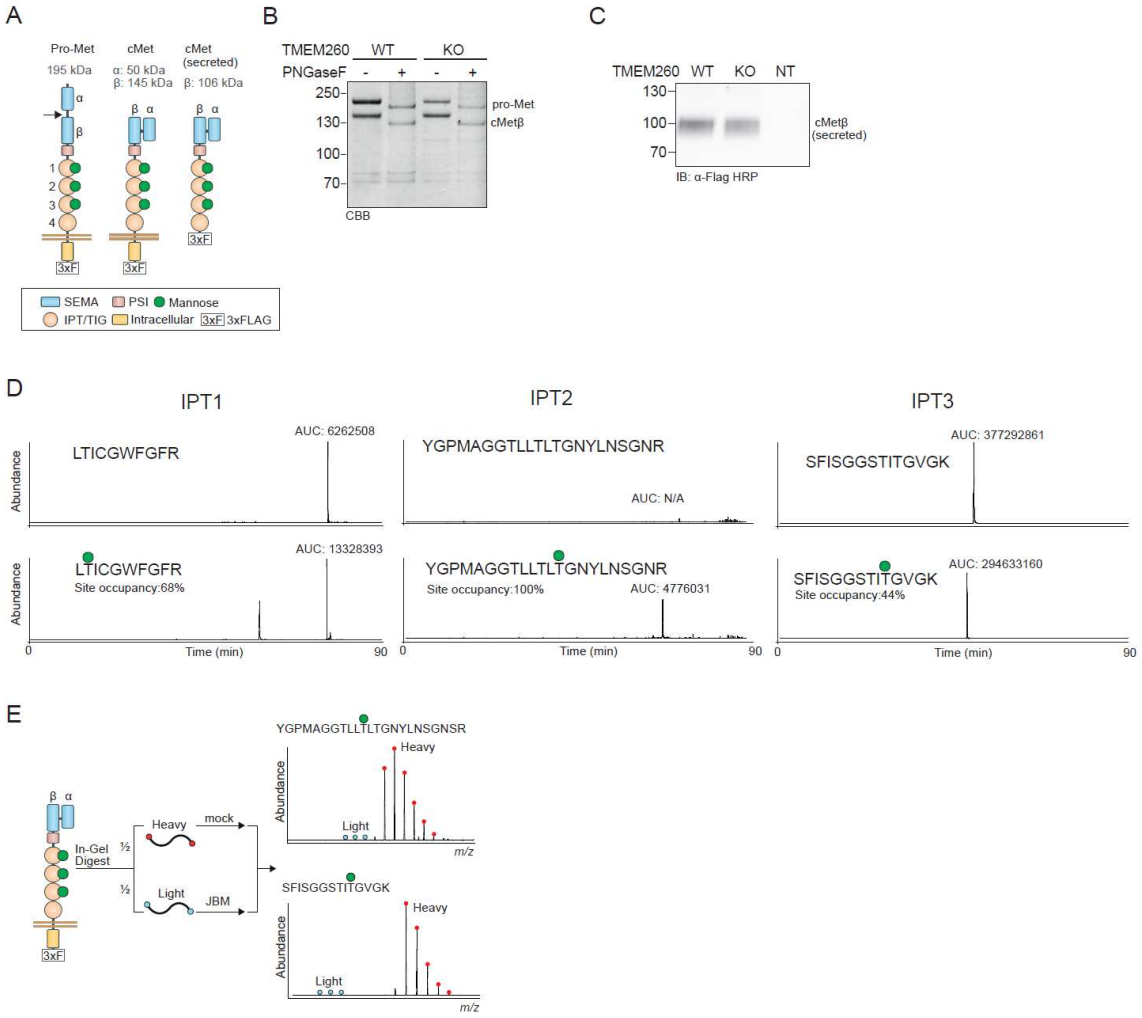

Fig. S5.

IPT domains of cMET are modified by alpha-linked O-Man glycans. **(A)** Graphical depiction of domain organization and pro-MET processing (arrow) into mature cMET α- and β-chains. O-Man modifications of IPT domains 1-3 is indicated by a filled green circle. The truncated cMET construct (secreted) is shown (right). **(B)** Affinity purified pro-Met and cMetβ from HEK293 cells resolved by SDS-PAGE analysis and visualized by coomassie protein stain. **(C)** Secreted cMetβ in cell culture media detected by western blot analysis of WT, TMEM260 KO and non-transfected (NT) HEK293 cells. **(D)** Extracted ion chromatograms of tryptic peptides and O-Man glycopeptides for sequences covering O-Man glycosylations sites of cMetβ IPT domains 1-3. Site occupancy is determined by integrating peak areas (AUC) of nLC elution profiles for each peptide and glycopeptide. Site occupancy (%) is calculated by (glycopeptide AUC / peptide+glycopeptide AUC)*100 for each sequence. The YGPMAGGTLLTLTGNYLNSGNR peptide was only detected with O-Man glycosylation and therefore calculated as fully (100%) occupied. **(E)** Workflow for diethyl stable isotope labeling and jack bean mannosidase (JBM) digestion of cMetβ peptides(left) together with relative quantification of heavy (red) and light (blue) labeled precursor ions corresponding to O-Man glycopeptides from cMetβ. The reduced abundance of light-labeled precursor ions demonstrates that O-Man glycans are sensitive to jack bean α-mannosidase treatment.

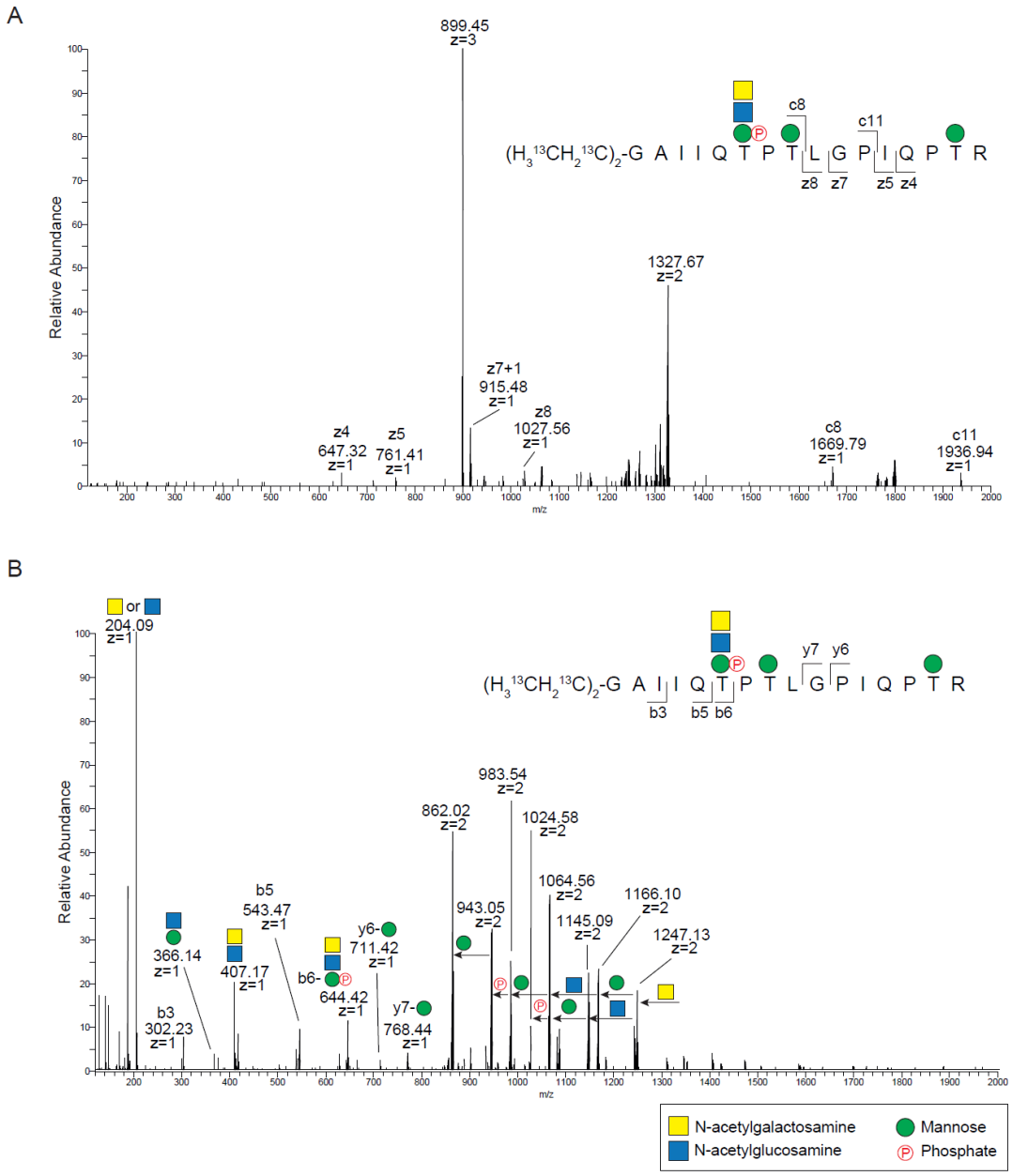

Fig. S6.

Unbiased mining of MS data with the open search MS Fragger tool. MS Fragger successfully identified complex O-Man glycosylations corresponding to phosphorylated core M3 on α-dystroglycan in ConA-LWAC enriched HEK293^{SC} total cell digests, but we did not find evidence supporting further elongation of O-Man on immunopurified pro-MET and cMETβ expressed in HEK293^{WT} cells, or on O-Man glycans of IPT domains enriched from total cell lysates. **(A)** ETciD fragmentation of the precursor ion (899.1101, z=3) matched to the heavy diethyl labelled GAIIQTPTLGPIQPTR tryptic peptide of α-dystroglycan with the Hex(3)HexNAc(2)Phosphate modification. **(B)** HCD fragmentation of the same precursor ion (899.1101, z=3) with characteristic oxonium ion fragments and neutral losses corresponding to Hex and HexNAc monosaccharides. MS2 spectra in (A) and (B) are partially annotated for clarity.

Table S1.

Summary of clinical features of two novel families with *TMEM260* deficiencies.

Family	**I**	**II**	
	Patient I	**Patient IIa**	**Patient IIb**
Age	5 years old boy	8 years old boy	Deceased 2 days old girl
Genotype	c.293 G>A, p. C98Y	c.1357 T>C, p. C453R	N/A
Cardiac defects	Truncus arteriosus, type II with an interrupted aortic arch type, aberrant R subclavian, and thymic hypoplasia	Truncus arteriosus, VSD, SD, tricuspid stenosis Cardiac surgery at 2 months	Truncus arteriosus and critical aortic stenosis
Kidneys defects	Kidneys are large for age bilaterally with pelvicaliectasis of the left kidney	Nephrocalcinosis bilaterally at 2 weeks old	N/A
Neurological defects	Global developmental delays	Global developmental delays	N/A
Face dysmorphism	Normal	Low-set ears	N/A
Speech	Non-verbal	Started speaking at 3.5 years	N/A
Autism	Diagnosed	N/A	N/A
Walking	2 years	2.5 years	N/A

Table S2.

Guide RNAs (gRNAs) used for genetic engineering.

Name	Species	Sequence
ghTMEM260_Exon3	Human	5’-TGGCTATCCTTTGTTCACGC-3’
gmTMEM260_Exon3	Mouse	5’-GTGAACAACGGATAGCCCGG-3’

Table S3.

Genetically engineered cell lines of this study.

Cell line	***Sanger sequence of TMEM260 locus***	***Indel generated***
HEK293^{WT}	5’-TGGCTATCCTTTGTTCACGCTGGTGGCTAAACTGGC-3’	WT
HEK293$^{SC/KO:TMEM260}$	5’-TGGCTATCCTTTGTTTCACGCTGGGCTAAACTGGC-3’	+1bp
HEK293$^{KO:TMEM260}$	5’-TGGCTATCCTTTGTTTCACGCTGGTGGCTAAACTGGC-3’	+1bp
BG1^{WT}	5’-TTTAGCCACCAGCGTGAACAAAGGATAGCCAGGAG -3’	WT
BG1$^{KO:TMEM260}$ #1	5’-TTTAGCCACCAGCGTGAAACAAAGGATAGCCAGGAG-3’	+1bp
BG1$^{KO:TMEM260}$ #2	5’ TTTAGCCACCAGCGTGAAACAAAGGATAGCCAGGAG-3’	+1bp
BG1$^{KO:TMEM260}$ #3	5’-TTTAGCCACCAGCGTGACAAAGGATAGCCAGGAG-3'	+1bp
mIMCD-3 ^{WT}	5’-TAGGTCGCCCATCCCCCGGGCTATCCGTTGTTCAC-3’	WT
mIMCD-3$^{KO:Tmem260}$ #1	5’-TAGGTCGCCCATCCCCCGGCTATCCGTTGTTCAC-3’	-1bp
mIMCD-3$^{KO:Tmem260}$ #2	5’-TAGGTCGCCCATCCCCCGGCTATCCGTTGTTCAC-3’	-1bp
Cell line	***Sanger sequence of TMTC3 locus***	***Indel generated***
BG1$^{KO:TMTC3}$	5’-TGTACTACTGCTGGACAGTTTCTTCCGTGGAAAGGGTAG-3’	+1bp

Table S4.

Primers for TMEM260 constructs and IDAA analyses**.**

Primers for mutagenesis of EPB71-TMEM260 WT 3xFLAG plasmid

Name	***Sequence***
phTMEM260_Q465*_Fwd	5’- AGTGGACTAAGAAATGATGACCTACG - 3’
phTMEM260_Q465*_Rev	5’- ATTTCTTAGTCCACTAAAGAAATGTCGG - 3’
phTMEM260_Y567Tfs*27_Fwd	5’- AACTGGACCGAGGAGTACGGAA - 3’
phTMEM260_Y567Tfs*27_Rev	5’- CTCCTCGGTCCAGTTATGGATTTTGTGAGCTTA - 3’
phTMEM260_C98Y_3xFLAG_Fwd	5’- GCTTATCGTGTGAATCTGCTCTATGGACTCTTCGGCGCTGTGGCC- 3’
phTMEM260_C98Y_3xFLAG_Rev	5’- GGCCACAGCGCCGAAGAGTCCATAGAGCAGATTCACACGATAAGC - 3’
phTMEM260_C453R_3xFLAG_Fwd	5’- TTCTTTAAGGTACATGCACTATCGTGAGGGATTACGTCCCGACAT - 3’
phTMEM260_C453R_3xFLAG_Rev	5’- ATGTCGGGACGTAATCCCTCACGATAGTGCATGTACCTTAAAGAA - 3’

Primers for 3xFLAG addition to EPB71-TMEM260 Q465* or Y567Tfs*27 plasmids

Name	**Sequence**
phTMEM260_Q465*_3xFLAG_Fwd	5’- CTTGTAGTCACCGCCGTCCACTAAAGAAATGTCGGGACG – 3’
phTMEM260_Y567Tfs*27_3xFLAG_Fwd	5’ – CTTGTAGTCACCGCCTACGAGCTTGCCACATCTCC - 3’
phTMEM260_Q465*/Y567Tfs*27_3xFLAG_Rev	5’ - GGCGGTGACTACAAGGACCAC – 3’

Primers for IDAA analyses

Name	**Species**	**Sequence**
phTMEM260_FwdEext	Human	5’-GCTGACCGGCAGCAAAATTGCCATGTGATAGACGCTGCCA-3’
phTMEM260_Rev	Human	5’-CATGTGTTAGGGAAACCAAGCAA-3’
pmTMEM260_FwdEext	Mouse	5’GCTGACCGGCAGCAAAATTGTAGGGAGCCACTGCCACTAT-3’
pmTMEM260_Rev	Mouse	5’AAATCACGTGACCGAGGGAC-3’

Table S5.

Antibodies used for Western Blot (WB), Immunofluorescence (IF) or FACS analysis.

Primary antibodies and chemicals

Antigen	Species	Vendor/cat. no.	Dilution	Application
Beta-Actin	Mouse	SCBT/SC-47778	1:3000; 5% milk in TBS-T	WB, Fig 1., Fig 2
E-cadherin	Mouse	BD/61018	1:200; 3% BSA in PBS	IF, Fig 3.
E-cadherin	Goat	R&D AF648	1:1000; 0.05% Saponin in PBS	Fig S3.
ERp57	Mouse	Ab13506	1:1000; 0.05% Saponin in PBS	IF, Fig 2.
cMET	Rabbit	CST/8198S	1:1000; 5% milk in TBS-T	WB, Fig.2
cMET	Rat	Invitrogen/14-8858-8	1:100; 1% FCS in PBS	FACS, Fig 2.
Calnexin	Rabbit	Enxo/ADI-SPA-860	1:1000; 0.05% Saponin in PBS	IF, Fig S3.
FLAG M2	Mouse	Sigma/F3165	1:300; 0.05% Saponin in PBS	IF, Fig S3, S5.
FLAG M2 HRP	Mouse	Sigma/A8592	1:5000; 5% milk in TBS-T	WB, Fig 1.
RON	Rabbit	CST/2654S	1:1000; 5% milk in TBS-T	WB, Fig 2.
RON	Mouse	BD/565691	1:100; 1% FCS in PBS	FACS, Fig 2.
Plexin-B2	Sheep	R&D/AF5329	1:1000; 5% milk in TBS-T, 1:500; 0.05% Saponin in PBS, 1:500; 1% FCS in PBS	WB, IF, FACS Fig 2.
TGN46	Rabbit	Abcam/ab505095	1:400; 0.05% Saponin in PBS	IF, Fig S3.
ZO-1	Rabbit	Invitrogen/617300	1:200; 3% BSA in PBS	IF, Fig 3.
DAPI		Sigma/D9542	1:5000; 0.05% Saponin in PBS, 3% BSA in PBS	IF, Fig 3.
7-ADD		Biolegend 420404	5 ul/sample; 1% FCS in PBS	FACS, Fig 2.

Secondary antibodies

Name	Vendor/cat. no.	Dilution	Application
Donkey anti-Mouse dylight 488	Invitrogen/SA5-10166	1:1000; 1% FCS in PBS	FACS, Fig 2.
Goat anti-Rat alexa 488	Invitrogen/A11006	1:1000; 1% FCS in PBS	FACS, Fig 2.
Donkey anti-Sheep alexa 488	Invitrogen/A11015	0.05% Saponin in PBS, 1:1000; 1% FCS in PBS	IF and FACS, Fig 2.
Donkey anti-Goat alexa 594	Invitrogen/A11058	1:1000; 0.05% Saponin in PBS	IF, Fig S3.
Donkey anti-Rabbit dylight 488	Invitrogen/SA5-10038	1:1000; 0.05% Saponin in PBS	IF, Fig S3.

Goat anti-Mouse alexa 488	Invitrogen/A11029	1:200; 3% BSA in PBS	IF, Fig 3.
Goat anti-Rabbit alexa 555	Invitrogen/A21429	1:200; 3% BSA in PBA	IF, Fig 3.
Polyclonal Rabbit anti-Mouse HRP	Dako/P0260	1:3000; 5% milk in TBS-T	WB, Fig 2A
Polyclonal Goat anti-Rabbit HRP	Dako/P0448	1:3000; 5% milk in TBS-T	WB, Fig 2A
Polyclonal Rabbit anti-Sheep HRP	Dako/P0163	1:3000; 5% milk in TBS-T	WB, Fig 2A

Data S1. (separate file)

Identification and quantification of relative abundances of O-Man glycopeptides enriched from total cell lysates. The experimental setup of paired (case and control) analyses of genetically engineered cell lines and their stable isotope coding is described. Results from each paired analyses can be found in individual sheets.

References (Supplementary information)

31. L. A. Lonowski *et al.*, Genome editing using FACS enrichment of nuclease-expressing cells and indel detection by amplicon analysis. *Nat Protoc* **12**, 581-603 (2017).
32. Z. Yang *et al.*, Fast and sensitive detection of indels induced by precise gene targeting. *Nucleic Acids Res* **43**, e59 (2015).
33. R. Pinto *et al.*, Precise integration of inducible transcriptional elements (PrIITE) enables absolute control of gene expression. *Nucleic Acids Res* **45**, e123 (2017).
34. P. J. Boersema, R. Raijmakers, S. Lemeer, S. Mohammed, A. J. Heck, Multiplex peptide stable isotope dimethyl labeling for quantitative proteomics. *Nat Protoc* **4**, 484-494 (2009).
35. J. Jung *et al.*, Deuterium-Free, Three-Plexed Peptide Diethylation for Highly Accurate Quantitative Proteomics. *J Proteome Res* **18**, 1078-1087 (2019).
36. Y. Perez-Riverol *et al.*, The PRIDE database resources in 2022: a hub for mass spectrometry-based proteomics evidences. *Nucleic Acids Res* **50**, D543-D552 (2022).
37. K. Retterer *et al.*, Assessing copy number from exome sequencing and exome array CGH based on CNV spectrum in a large clinical cohort. *Genet Med* **17**, 623-629 (2015).
38. M. Lommel, A. Schott, T. Jank, V. Hofmann, S. Strahl, A conserved acidic motif is crucial for enzymatic activity of protein O-mannosyltransferases. *J Biol Chem* **286**, 39768-39775 (2011).
39. M. B. Lazarus, Y. Nam, J. Jiang, P. Sliz, S. Walker, Structure of human O-GlcNAc transferase and its complex with a peptide substrate. *Nature* **469**, 564-567 (2011).

Supplementary Files

This is a list of supplementary files associated with this preprint. Click to download.

- DatasetS1.xlsx